metals

MDPI

Article

Microstructure Evolution and Properties of β-TCP/Mg-Zn-Ca Biocomposite Processed by Hot Extrusion Combined with Multi-Pass ECAP

Xiaohao Sun [1], Yue Su [1], Yan Huang [2], Minfang Chen [3] and Debao Liu [4,*]

[1] School of Materials Science and Engineering, Tianjin University of Technology, Tianjin 300384, China; kwindyd@gmail.com (X.S.); yuesutemp@163.com (Y.S.)
[2] Brunel Centre of Advanced Solidification Technology (BCAST), Brunel University London, Uxbridge, London UB8 3PH, UK; yan.huang@brunel.ac.uk
[3] Tianjin Key Laboratory for Photoelectric Materials and Devices, Tianjin University of Technology, Tianjin 300384, China; mfchentj@126.com
[4] National Demonstration Center for Experimental Function Materials Education, Tianjin University of Technology, Tianjin 300384, China
* Correspondence: debaoliu@126.com

Abstract: To further improve the comprehensive performance of Mg-based alloy, hot extrusion combined with multi-pass equal channel angular pressing (ECAP) was applied to process Mg-3 wt%Zn-0.2 wt%Ca alloy and 1 wt%β-TCP/Mg-3 wt%Zn-0.2 wt%Ca biocomposites. The microstructure evolution, mechanical properties, corrosion behavior, and cell biocompatibility of the experimental specimens were systematically investigated. The average grain size of 13.4 ± 0.6 μm in MgZnCa alloy and 9.6 ± 0.3 μm in composites materials can be achieved by six ECAP passes. The uniaxial compressive strength (UCS) of 388.4 ± 7.3 MPa and the strain at failure of 14.3 ± 1.5% were confirmed in MgZnCa alloy, while the UCS of 405.3 ± 7.4 MPa and the strain at failure of 9.8 ± 1.9% were achieved by the addition of β-TCP after six ECAP passes. In spite of different compositions, the minimum corrosion rate of 0.895 mm·Y^{-1} and 1.117 mm·Y^{-1} can be achieved by two ECAP passes at 593 K. The cytocompatibility evaluation revealed that the experimental materials processed by six ECAP passes had no significant cytotoxicity to L929 cells, and the addition of β-TCP improved the cytocompatibility.

Keywords: magnesium-based composites; equal channel angular pressing; microstructure; mechanical properties; corrosion resistance; biocompatibility

Citation: Sun, X.; Su, Y.; Huang, Y.; Chen, M.; Liu, D. Microstructure Evolution and Properties of β-TCP/Mg-Zn-Ca Biocomposite Processed by Hot Extrusion Combined with Multi-Pass ECAP. *Metals* **2022**, *12*, 685. https://doi.org/10.3390/met12040685

Academic Editor: Leszek Adam Dobrzanski

Received: 25 March 2022
Accepted: 14 April 2022
Published: 16 April 2022

1. Introduction

Biodegradable magnesium (Mg)-based materials attracted significant attention for their potential application in the biomedical industry [1,2]. Compared with conventional metallic biomaterials such as stainless steel [3], CoCr [4], and titanium alloys [5], biodegradable Mg alloys can be safely metabolized after fulfilling their function in the human body, which circumvents secondary operation for the removal of the implant. By using biodegradable Mg-based implant materials, the burden on the body and the economy of the patients could be decreased [6]. Moreover, compared to the bioinert metallic materials, Mg-based materials possess lower densities of 1.74–2.00 g·cm^{-3}, and a lower elastic modulus of 10–40 GPa [7,8]. It is beneficial to reduce the stress shielding effect after Mg alloys are implanted in the human body [8]. Among various Mg-based alloy systems, the Mg-Zn-Ca alloys have been recognized as promising candidates for orthopedic applications due to their biodegradability and good biocompatibility [9–12]. Zn as the alloying element could enhance the corrosion resistance of the Mg matrix by forming a compound protective layer on the material's surface, while Ca shows excellent biocompatibility like Mg, and is prone to form calcium phosphate during degradation, which is beneficial to the formation

of bone tissue [13,14]. Furthermore, the development of magnesium-matrix composites reinforced by bioactive ceramics could be an efficiency approach to further improve the mechanical performance further and functionalize materials simultaneously [15–17]. In previous studies, beta-tricalcium phosphate (β-TCP), which is a bioactive ceramic, was used to develop β-TCP/Mg-Zn-Ca biocomposites with [18–20]. However, before the appropriate post-treatment, the mechanical performance of these composites is still insufficient to meet the requirement of a load-bearing orthopedic implant.

Generally, the plastic formation process is necessary to improve the mechanical performance of Mg-based materials and a conventional hot extrusion process was widely used for this purpose [21–23]. However, conventional extrusion is a single-pass plastic formation process, making it hard to provide sufficient deformation to achieve an adequate and controllable mechanical performance. On the contrary, the ECAP process could provide a cumulative shear strain without changing the cross-sectional area of the processed materials. In other words, unlike the conventional extrusion process, the ECAP process could be repeated multiple times, contributing to a significant plastic strain and substantial grain refinement in the ECAP-processed materials [24–28]. In recent years, several studies regarding the feasibility of the ECAP process for controlling the microstructure and mechanical properties of Mg-based composites were reported. Significant grain refinement effects caused by multi-pass ECAP were confirmed in AZ31, AZ61, and AZ91-based materials [29–32]. In the meantime, the ECAP process could simultaneously ameliorate the strength and ductility of Mg-based composites. Moreover, Gan et al. [33] reported the re-distribution of reinforcements particles in the Mg_2Si/Mg composites after the ECAP process, resulting in a homogeneous distribution of Mg_2Si reinforcements. More importantly, the ECAP process also could adjust the corrosion resistance of Mg-based alloy by grain refinement and the redistribution of second phases [34]. However, scant reports are available to the best of our knowledge, exploring the feasibility of the conventional extrusion combined with the multi-pass ECAP process for the Mg-based composite. Furthermore, the evolution of microstructure, mechanical properties, and corrosion behavior of β-TCP/Mg-Zn-Ca biocomposites during the ECAP process was still unclear.

In the present study, the 1β-TCP/Mg-3Zn-0.2Ca composite has been fabricated by casting with high-speed stirring and ultrasonication followed by a conventional hot extrusion process. Thereafter, a multi-pass ECAP process was performed for the 1β-TCP/Mg-3Zn-0.2Ca composites. The microstructure evolution, mechanical properties, corrosion behavior, and cytocompatibility of ECAP-processed 1β-TCP/Mg-3Zn-0.2Ca composites were systematically investigated. The comprehension effect of conventional extrusion combined with the ECAP process as a promising approach for the development of 1β-TCP/Mg-3Zn-0.2Ca composites was evaluated and discussed in detail.

2. Materials and Methods

2.1. Material Preparation Method

Commercially available high-purity magnesium ingots (99.99 wt%), pure zinc granules (99.99 wt%) with the size of 3–4 mm, magnesium-calcium intermediate alloy (25 wt% Ca) and β-TCP nanoparticles were used as raw materials. β-TCP particles with an average diameter of ~150 nm were prepared via a hydrothermal method, which was reported elsewhere [35]. Generally, compared with micro-sized TCP particles, nano-sized counterparts with the same content could result in a higher specific surface area and a higher number density in the Mg matrix, which could possibly induce a more intimate bonding between TCP and Mg matrix, and a more efficient grain refinement effect [36–38]. Furthermore, nano-reinforcements can remarkably increase mechanical strength by effectively promoting particle hardening mechanisms [39]. Hence, for the sake of efficient grain refinement and effective strengthening behavior, nano-sized β-TCP particles were chosen as the reinforcement for the Mg-Zn-Ca matrix. According to our experience, to achieve a substantial improvement in mechanical performance and avoid the aggregation of β-TCP particles, the β-TCP content was set at 1 wt%. A schematic diagram of the processing route of Mg-3Zn-

0.2Ca alloy and 1β-TCP/Mg-3Zn-0.2Ca composite is shown in Figure 1a. A self-developed furnace with the devices for high-speed stirring and ultra-sonication was employed for the material preparation. Under the protective atmosphere of N_2 + SF_6, the raw materials were melted at 993 K under high-speed stirring and ultra-sonication for 15 min and then cast. Subsequently, the ingot was hot extruded into a square rod with an edge length of 15 mm followed by a multi-pass ECAP process with an internal-channel angle of 120° and an external angle of 0°, as shown in Figure 1b. The specimens were preheated for 15 min before each ECAP pass. The ECAP process was carried out in route A (no rotation between subsequent passes) with a cross-head speed of 2 mm·s^{-1}.

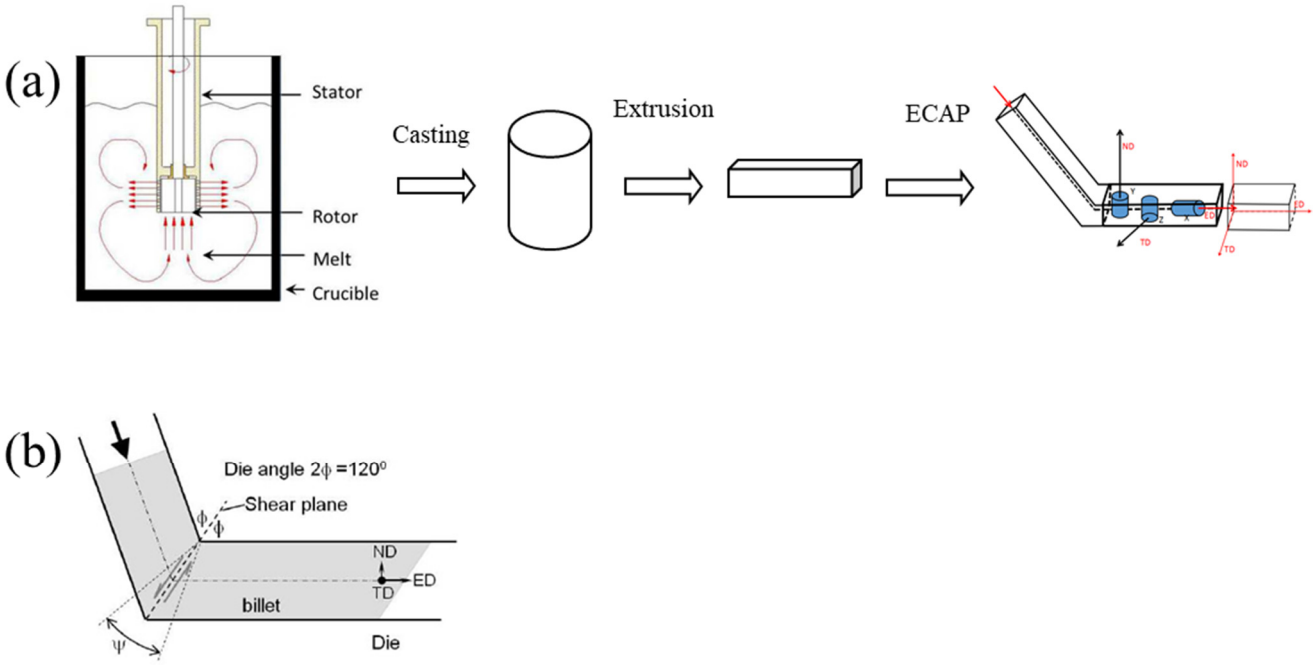

Figure 1. Schematic diagram of (**a**) the processing route of Mg-3Zn-0.2Ca alloy and 1β-TCP/Mg-3Zn-0.2Ca composite; (**b**) the essential geometrical parameters for the ECAP die and specimen orientation nominations.

In this study, the ECAP processing parameters for Mg-3Zn-0.2Ca alloy and the 1β-TCP/Mg-3Zn-0.2Ca composites were summarized in Table 1. The ECAP-processed specimens were named using composition (A means Mg-3Zn-0.2Ca alloy and C means 1β-TCP/Mg-3Zn-0.2Ca composite), ECAP processing times, and ECAP temperature for convenience. For example, A-2-593 K means that Mg-3Zn-0.2Ca alloy ECAP was treated 2 times at 593 K. The effect of ECAP on the microstructure mechanical properties and corrosion resistance of the materials was systematically investigated from the ED of the experimental specimens.

Table 1. ECAP processing parameters used in this study.

Names	Material	ECAP Times	Temperature (K)
A-as-extruded	alloy	0	-
C-as-extruded	composite	0	-
A-2-593 K	alloy	2	593
C-2-593 K	composite	2	593
A-4-593 K	alloy	4	593
C-4-553 K	composite	4	553

Table 1. *Cont.*

Names	Material	ECAP Times	Temperature (K)
C-4-573 K	composite	4	573
C-4-593 K	composite	4	593
C-4-613 K	composite	4	613
A-6-593 K	alloy	6	593
C-6-593 K	composite	6	593
A-8-593 K	alloy	8	593
C-8-593 K	composite	8	593

2.2. Phase Analysis and Microstructure Observation

The phase constitution was analyzed by X-ray diffraction (XRD; SmartLab, Rigaku, Tokyo, Japan) using Cu-Ka radiation (k = 0.154059 nm) with an operating voltage of 40 kV and an operating current of 44 mA. XRD investigation was carried out over the 2 theta range of 20° to 80° with a step size of 0.02° and a dwelling time of 1 s. The test surface was perpendicular to the extrusion direction. The microstructure observations were performed on an optical microscope (GX51, OLYMPUS, Tokyo, Japan). The grain size was measured using an automatic image analyzer (OLYMPUS M3, OLYMPUS, Tokyo, Japan), using the linear intercept method as described in the ASTM standard E112-G6. Transmission electron microscope (TEM) investigations were performed on a JEOL 2100 device (JEOL, Tokyo, Japan) at an accelerated voltage of 200 kV. The TEM specimens were prepared by twin-jet etching by a mixed solution of 2.75 g picric acid, 2.5 mL glacial acetic acid, 5 mL deionized water, and 45 mL anhydrous ethanol. Texture analysis for the C-as-extruded and the C-4-593 K was executed by electron backscatter diffraction (EBSD; Hikari XP, EDAX, Mahwah, NJ, USA). The samples for EBSD were prepared by a typical ion-milling method. The EBSD results were analyzed using the Channel 5 software (Version 3.1, Hobro, Denmark).

2.3. Mechanical Properties

The mechanical properties were tested via compressive test. Samples for the compressive tests are processed into the dimension of Φ 4 mm × 8 mm. The compression rate was 0.5 mm·s^{-1}. The compressive yield strength was determined according to ASTM E111. Three parallel samples were tested for each material.

2.4. Electrochemical Measurements

Electrochemical analysis was performed at 310 K using an electrochemical workstation (Zennium Zahner, Sciencetech, London, ON, Canada), which consisted of the electrolytic tank containing simulated body fluid (SBF) and a standard three-electrode system (graphite as the control electrode, saturated calomel electrode as the reference electrode and the sample as the working electrode). After the open circuit potential was recorded for 1800 s, the potential dynamic polarization was performed at a scanning rate of 1 mV·s^{-1}, and the voltage range was set as self-corrosion potential ± 500 mV.

2.5. Cell Biocompatibility Evaluation

The test was determined pursuant to ISO 10993-5 standard [40]. The medium was RPMI-1640 (Thermo Fisher Scientific, Waltham, MA, USA) supplemented with 10% inactivated fetal bovine serum, 100 U·mL^{-1} penicillin, and 100 U·mL^{-1} streptomycin. Samples (7 mm × 7 mm × 3 mm) were sterilized by ultraviolet rays, and then added into RPMI-1640 culture medium according to the ratio of sample surface area to culture volume of 3 cm^2·mL^{-1}, and placed in an incubator with 5% CO_2 at 310 K for leaching for 7 days to obtain the leaching stock solution. Mouse fibroblasts (L-929 cells) were grown in a cell culture incubator with 5% CO_2 at 310 K. Four parallel samples were set for each material in this test. The negative control group was 10% serum +90% RPMI-1640 culture medium. 100 mL cells were stained with 0.4% trypan blue. According to the concentration of 5000 cells·well-1, the cells were injected into a 96-well culture plate and cultured at 310 K for 24 h, then washed

with phosphate buffer solution (PBS). After 1 day, 3 days, and 5 days of culture, the cells were taken out, and 20 mL 3-(4, 5-Dimethylthiazol-2-yl)-2, 5-diphenyltetrazolium bromide (MTT) with a concentration of 5 mg·mL-1 was added to continue to culture for 3 h. After MTT fully reacted with the cells, the supernatant of the culture medium was removed, and 150 mL dimethyl sulfoxide was added. After the crystals were completely dissolved, the absorbance (OD value) was measured with a microplate reader at a wavelength of 570 mm. The relative proliferation rate of the cells was calculated as RGR (average OD of the experimental group × 100%/mean OD of the negative control group).

3. Results and Discussion

3.1. Phase Analysis

Figure 2 shows the XRD profiles of as-extruded Mg-3Zn-0.2Ca alloy and 1β-TCP/Mg-3Zn-0.2Ca composite. For A-as-extruded and C-as-extruded, the main constitution was identified as the α-Mg, the second phases were composed of $Ca_2Mg_6Zn_3$ and MgZn phases. However, no diffraction peak of TCP was detected by XRD in the C-as-extruded. It may be because the β-TCP content is lower than the sensitive value detected by XRD. No diffraction peak of the intermediate phase between the β-TCP and the matrix alloy was identified in the C-as-extruded, indicating that no significant chemical reaction occurred between β-TCP and the matrix alloy.

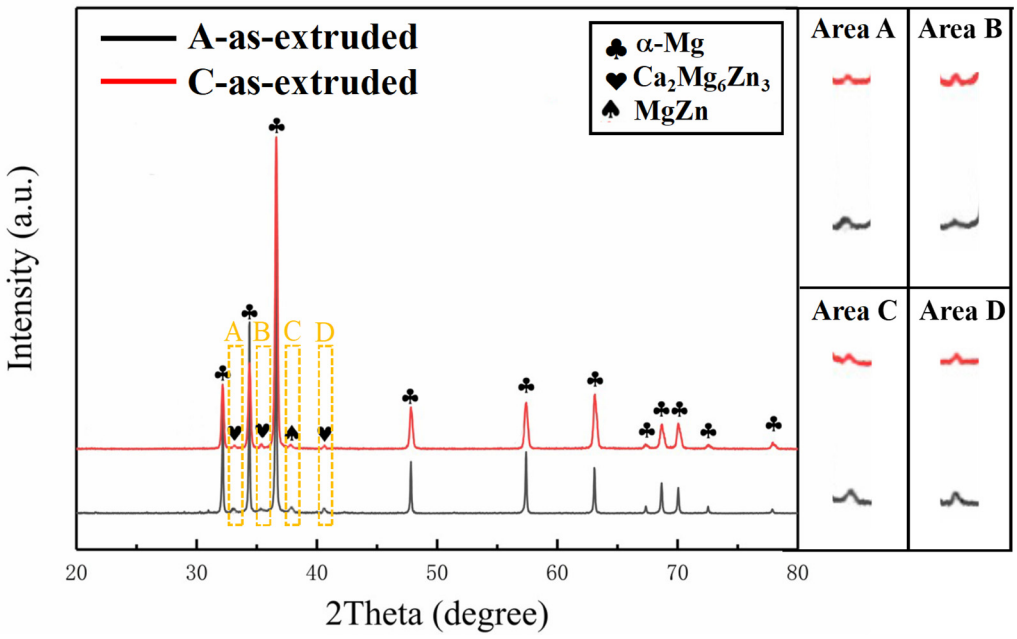

Figure 2. XRD profiles of A-as-extruded and C-as-extruded specimens.

3.2. Microstructure Observation

Figure 3 shows the microstructure of as-cast, as-extruded and different ECAP passes (0, 2, 4, 6, and 8) at 593 K of Mg-3Zn-0.2Ca alloy and 1β-TCP/Mg-3Zn-0.2Ca composites. Compared with the as-cast microstructure of Mg-3Zn-0.2Ca alloy as shown in Figure 3a, the as-extruded alloy exhibits significant grain refinement. Equiaxed morphology was observed in as-extruded and ECAP-processed specimens. When the ECAP times up to two, the Mg-3Zn-0.2Ca alloy exhibits apparent grain refinement compared with the as-extruded. With the further increase in ECAP passes, the grain refinement effect of Mg-3Zn-0.2Ca alloy is enhanced. The A-6 P-593 K possesses the smallest grain size. When the ECAP times were more than six (eight in this study), it is apparent that some grains grow excessively. The average grain sizes of Mg-3Zn-0.2Ca alloy components with 0, 2, 4, 6, and 8 ECAP passes are approximately 17.1 ± 1.3 mm, 15.6 ± 1.0 mm, 14.4 ± 0.8 mm, 13.4 ± 0.6 mm and 14.2 ± 0.8 mm, respectively.

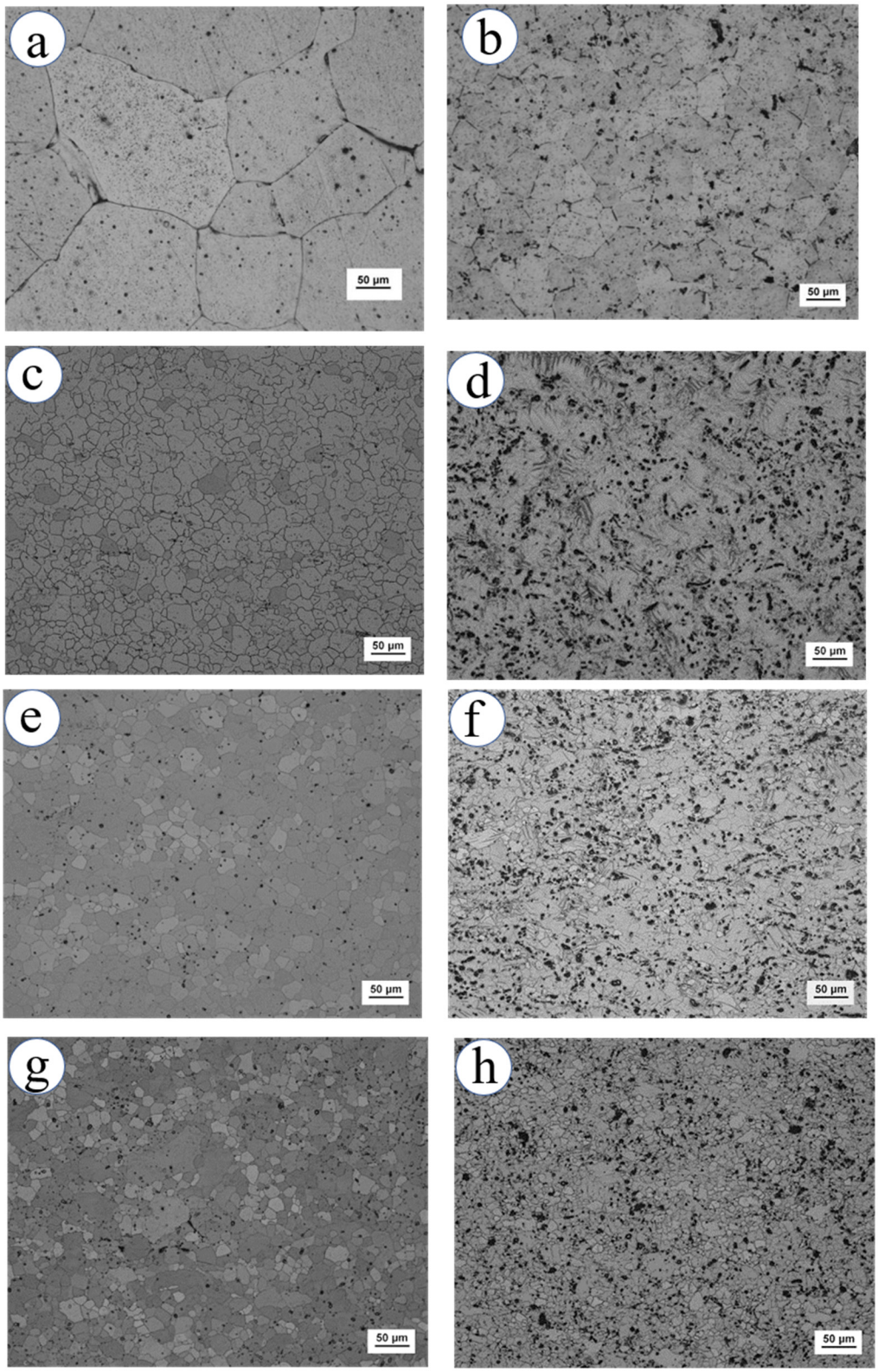

Figure 3. *Cont.*

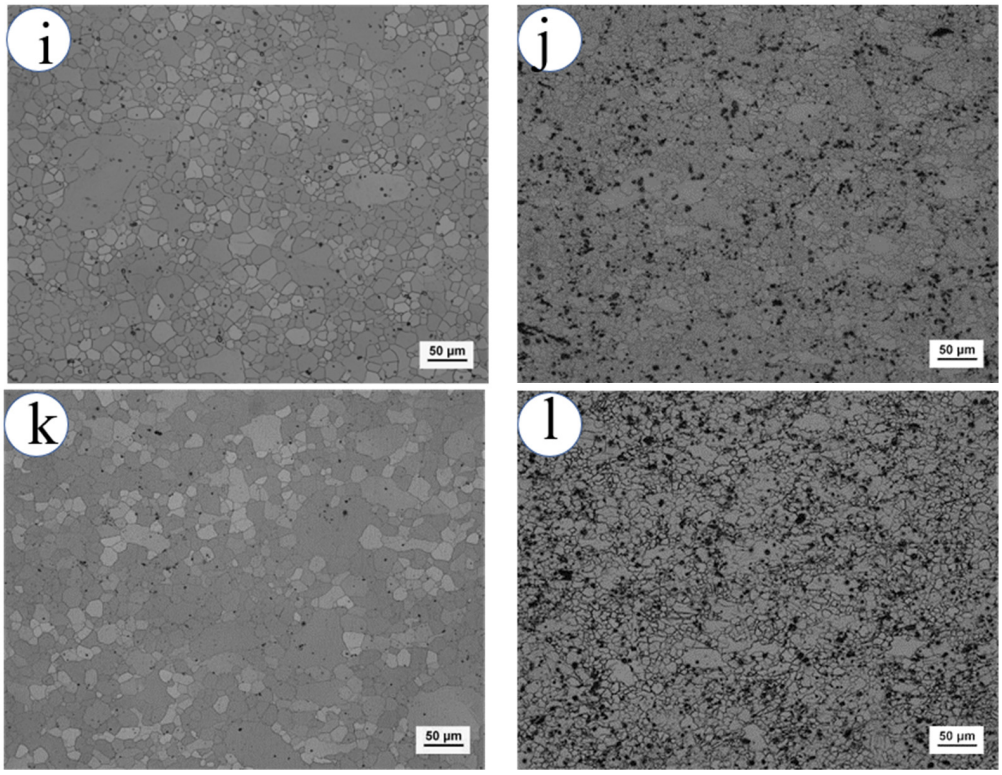

Figure 3. The microstructure of as-cast and ED surface of Mg-3Zn-0.2Ca alloy and 1β-TCP/Mg-3Zn-0.2Ca composites: (**a**) A-as-cast, (**b**) C-as-cast, (**c**) A-as-extruded, (**d**) C-as-extruded, (**e**) A-2 P-593 K, (**f**) C-2 P-593 K, (**g**) A-4 P-593 K, (**h**) C-4 P-593 K, (**i**) A-6 P-593 K, (**j**) C-6 P-593 K, (**k**) A-8 P-593 K, (**l**) C-8 P-593 K.

Similarly, compared with the as-cast microstructure of 1β-TCP/Mg-3Zn-0.2Ca composite as shown in Figure 3b, the as-extruded composite also shows significant grain refinement. The average grain sizes of 1β-TCP/Mg-3Zn-0.2Ca composites after 0, 2, 4, 6 and 8 ECAP passes processing are approximately 13.4 ± 1.1 mm, 11.6 ± 0.9 mm, 10.8 ± 0.5 mm, 9.6 ± 0.3 mm and 10.4 ± 0.5 mm, respectively. It is worth noting that 1β-TCP/Mg-3Zn-0.2Ca composite possessed smaller average grain sizes than the Mg-3Zn-0.2Ca alloy processed by the same ECAP parameters. This is mainly due to the role of β-TCP particles in facilitating the dynamic recrystallization and hindering the grain growth during the ECAP process. It is worth noting that the dispersion properties of β-TCP were improved after the ECAP process, due to the redistribution of β-TCP caused by significant shear deformation. The microstructure evolution of the experiment materials with multiple ECAP passes can be partially attributed to the dynamic recrystallization and the redistribution of second phases and β-TCP particles. Under the strong shear force derived from the ECAP process, the Mg-3Zn-0.2Ca alloy undergoes severe plastic deformation in each ECAP processing. The severe plastic deformation caused dynamic recrystallization and promoted grain refinement. In the meantime, the redistribution of the second phase would occur in each ECAP processing due to the strong shear force of ECAP. Figure 4 shows TEM images and corresponding EDS results for the second phase which should be the $Ca_2Mg_6Zn_3$ phase. However, when the ECAP times were beyond six (eight in this study), the factor of recovery dominated the microstructure evolution of A-8 P-593 K, thereby facilitating the grain growth, resulting in higher grain size than that of A-6 P-593 K specimens. In the case of 1β-TCP/Mg-3Zn-0.2Ca biocomposites, except for the grain refinement and redistribution of $Ca_2Mg_6Zn_3$ s phase, the dispersion properties of the β-TCP particles were also improved under the substantial deformation derived from the ECAP process. The improved dispersion properties of β-TCP are also beneficial to grain refinement by hindering the movement of grain boundary and acting as a potential nucleation site. Therefore, from the viewpoint of grain refinement,

six ECAP passes at 593 K should be the optimal ECAP parameter for Mg-3Zn-0.2Ca alloy and 1β-TCP/Mg-3Zn-0.2Ca composite.

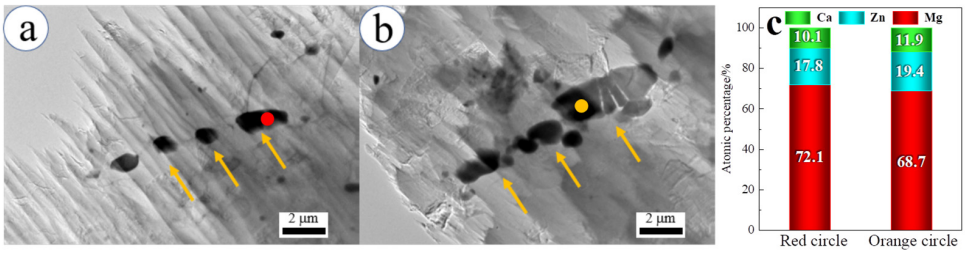

Figure 4. TEM images for the $Ca_2Mg_6Zn_3$ phase in the Mg-3Zn-0.2Ca alloy and 1β-TCP/Mg-3Zn-0.2Ca composite: (**a**) A-6 P-593 K, (**b**) C-6 P-593 K; (**c**) EDS point analysis results derived from red solid circle in (**a**) and orange solid circle in (**b**) (Orange arrows refers to the $Ca_2Mg_6Zn_3$ s phases).

On the other hand, ECAP temperature also obviously impacts the microstructure of 1β-TCP/Mg-3Zn-0.2Ca composites. Figure 5 shows the microstructure of the as-extruded 1β-TCP/Mg-3Zn-0.2Ca composites processed by 4 ECAP passes at different temperatures (553 K, 573 K, 593 K, and 613 K). When the 1β-TCP/Mg-3Zn-0.2Ca composite was processed at 553 K, coarse grains and small grains coexisted to form a heterogeneous microstructure, as shown in Figure 5a. With the further increase in ECAP temperature, the volume fraction of refined grains increased. When the ECAP temperature was up to 593 K, the C-4 P-593 K displayed the most uniform microstructure. According to Figure 5d, when the ECAP temperature was up to 613 K, abnormal grain growth was observed due to the excessive temperature. The average grain sizes of C-4 P-553 K, C-4 P-573 K, C-4 P-573 K, and C-4 P-613 K are approximately 9.8 ± 0.9 mm, 10.3 ± 0.8 mm, 10.8 ± 0.5 mm and 11.1 ± 0.7 mm, respectively. The increase in ECAP temperature was beneficial to the dislocation slip and plastic deformation of the 1β-TCP/Mg-3Zn-0.2Ca composite, which means that the uniform microstructure could be achieved. On the other hand, the increase in ECAP temperature accelerated grain growth of 1β-TCP/Mg-3Zn-0.2Ca composites [40], which was adverse to grain refinement. Hence, due to the competitive effect of grain growth and recrystallization, the C-4 P-593 K displayed the most uniform microstructure among all specimens with different ECAP temperatures.

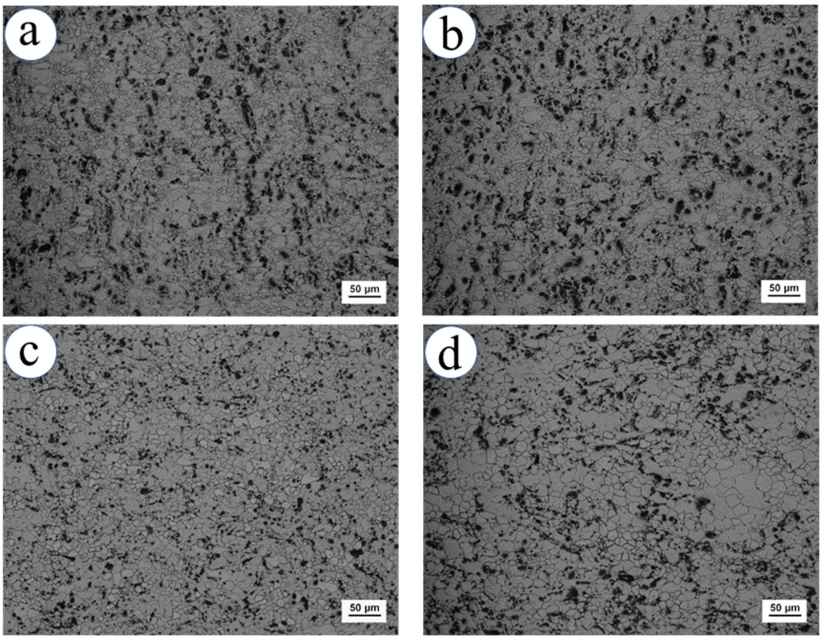

Figure 5. The ED surface microstructure of 1β-TCP/Mg-3Zn-0.2Ca composite: (**a**) C-4 P-553 K, (**b**) C-4 P-573 K, (**c**) C-4 P-593 K, (**d**) C-4 P-613 K.

From the viewpoint of microstructure, 593 K should be the optimal temperature of the ECAP process for the 1β-TCP/Mg-3Zn-0.2Ca composites.

3.3. Texture Evolution

Figure 6 provides the inverse pole figures, the misorientation angle distributions, and the grain size distributions of the C-as-extruded and the C-6 P-593K specimens. According to Figure 6a,b, a heterogeneous microstructure was formed in an as-extruded composite, including the coarse grains whose grain sizes are larger than 60 um and fine grains whose grain sizes are under 5 um. After six passes of ECAP processing, almost all elongated grains in as-extruded specimens were transformed into fine recrystallized grains, reducing the average grain size. Grain size distribution results reveal that a relatively narrow distribution was achieved in C-6 P-593 K compared with as-extruded counterparts, which means the ECAP process contributes to the homogenization of microstructure, as shown in Figure 6d,e. This is mainly due to ECAP-induced dynamic recrystallization, and the redistribution of the second phase and β-TCP particles. As shown in Figure 6c,f, the proportion of high angle grain boundaries (HAGBs) of the C-6 P-593 K increases compared with that of the C-as-extruded 1β-TCP/Mg-3Zn-0.2Ca composite, which is a key character of dynamic recrystallization.

Figure 7 shows the (0 0 0 1) pole Figures of the C-as-extruded and the C-6 P-593 K. The C-as-extruded possessed a single (0 0 0 1) texture, in which the (0 0 0 1) basal plane paralleled to ED-axis. The texture is typical for magnesium alloys processed by hot extrusion [33]. The texture of the C-6 P-593 K changed and was divided into two kinds of texture. One, which corresponds to area A in Figure 7b, indicates the (0 0 0 1) basal plane parallel to the ND plane. The other one, which corresponds to area B in Figure 7b, indicates that the angle between the normal direction of (0 0 0 1) basal plane and the ED-axis is 60 degrees. It is supposed that the substantial shear stress, which also possessed an angle of 60 degrees with the ED-axis, contributes to the formation of the second texture type during the ECAP process.

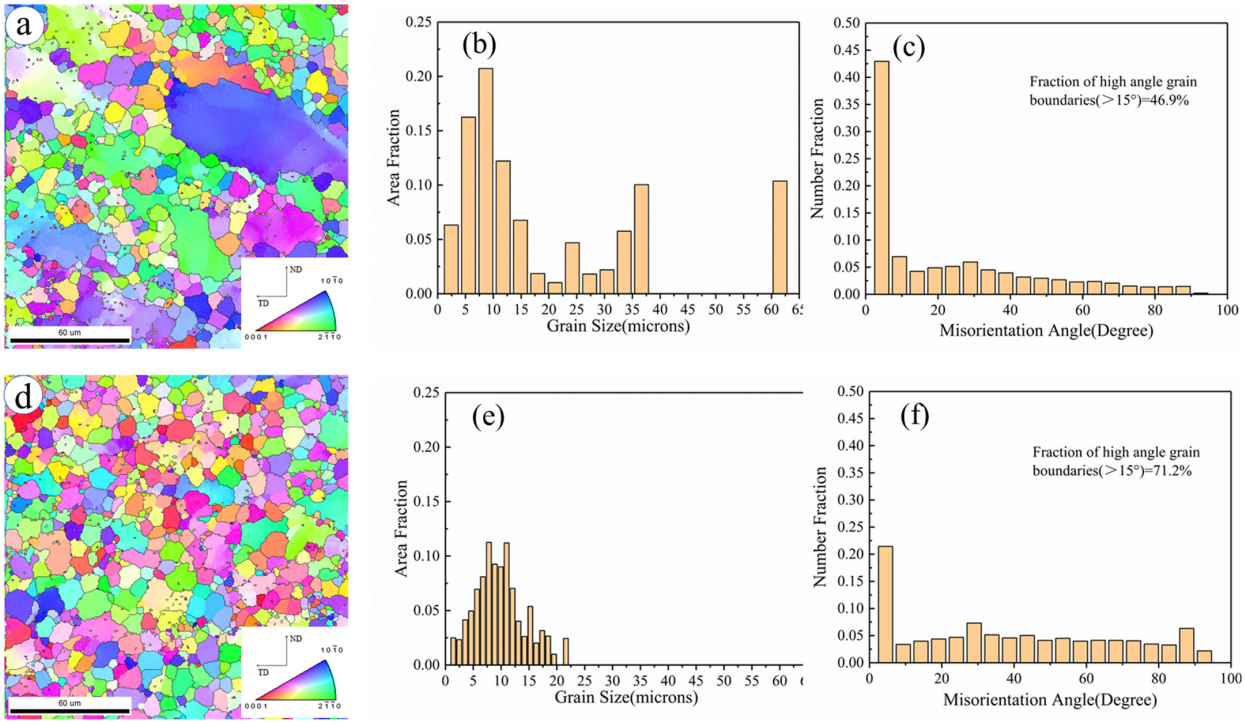

Figure 6. (**a**,**d**)The inverse pole figures, (**b**,**e**) misorientation angle distributions, and (**c**,**f**) grain size distributions of (**a**–**c**) the C-as-extruded and (**d**–**f**) the C-6 P-593 K.

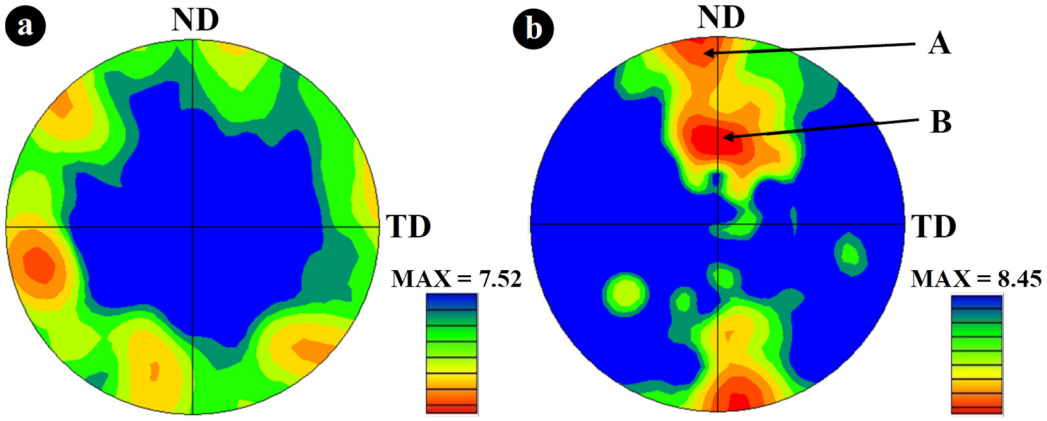

Figure 7. The (0 0 0 1) pole figures for α-Mg phase in (**a**) C-as-extruded and (**b**) C-6 P at 593 K.

3.4. Mechanical Properties

Figure 8 shows the compressive stress–strain curves of Mg-3Zn-0.2Ca alloy and 1β-TCP/Mg-3Zn-0.2Ca with different ECAP process parameters. The results of the compressive test (UCS, CYS, and strain at failure (σ)) are shown in Table 2.

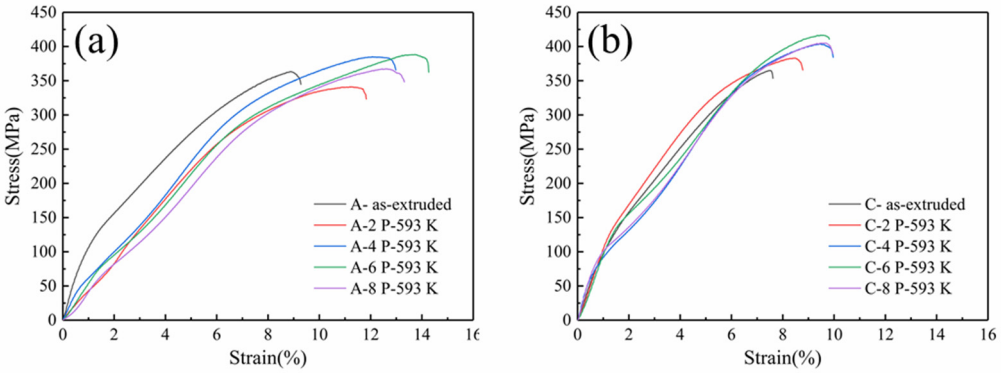

Figure 8. Compressive stress–strain curves of (**a**) Mg-3Zn-0.2Ca alloy and (**b**) 1β-TCP/Mg-3Zn-0.2Ca composites with different ECAP process parameters.

Table 2. Summary of mechanical properties of the experimental specimens.

Name	UCS (MPa)	CYS (MPa)	σ (%)
A-as-extruded	360.6 ± 8.5	103.1 ± 6.4	9.5 ± 1.5
C-as-extruded	365.9 ± 9.3	107.8 ± 5.8	7.6 ± 1.3
A-2 P-593 K	341.1 ± 6.4	75.7 ± 6.1	11.9 ± 2.0
C-2 P-593 K	382.5 ± 7.6	112.4 ± 6.3	8.8 ± 1.7
A-4 P-593 K	384.9 ± 9.5	84.6 ± 5.7	13.0 ± 1.9
C-4 P-593 K	405.3 ± 7.4	118.9 ± 7.0	9.8 ± 1.9
A-6 P-593 K	388.4 ± 7.3	94.5 ± 7.2	14.3 ± 1.5
C-6 P-593 K	411.7 ± 6.8	123.6 ± 5.5	10.1 ± 2.8
A-8 P-593 K	367.1 ± 8.1	86.8 ± 8.7	13.4 ± 2.3
C-8 P-593 K	401.0 ± 6.9	115.7 ± 7.1	9.4 ± 1.8

For Mg-3Zn-0.2Ca alloy, it was found that both strength and strain at failure of Mg-3Zn-0.2Ca alloy increase first and then decrease with the increasing ECAP passes. The A-6 P-593K exhibits the optimized mechanical performance in Mg-3Zn-0.2Ca alloy groups, which includes the UCS of 388.4 ± 7.3 MPa, and the CYS of 94.5 ± 7.2 MPa, and the strain at failure of 14.3 ± 1.5%. For 1β-TCP/Mg-3Zn-0.2Ca composites groups, the C-6 P-593K specimens showed the best comprehensively mechanical performance, including the UCS of 411.7 ± 6.8 MPa, the CYS of 123.6 ± 5.5 MPa and the strain at failure of 10.1 ± 2.8%.

Thus, the optimal ECAP parameter for Mg-3Zn-0.2Ca alloy and 1β-TCP/Mg-3Zn-0.2Ca composite should be six ECAP passes at 593 K from the viewpoint of mechanical properties. It is worth mentioning that 1β-TCP/Mg-3Zn-0.2Ca composites possess higher strength but lower strain at failure than the Mg-3Zn-0.2Ca alloy components processed by the same ECAP parameters. This may be due to the improved dispersion properties of β-TCP particles induced by the severe shear force during the ECAP process. Furthermore, β-TCP particles could facilitate nucleation during the ECAP process, thereby contributing to the recrystallization and grain refinement in the ECAP-process composites. Above all, the improved mechanical performance of ECAP-processed 1β-TCP/Mg-3Zn-0.2Ca composites is associated with enhanced second phase strengthening and grain refinement strengthening caused by uniformly dispersed β-TCP particles and β-TCP-induced recrystallization.

The enhanced mechanical properties of the ECAP-processed 1β-TCP/Mg-3Zn-0.2Ca composites could be explained as follows. According to the Hall–Petch relationship, grain refinement induced by the ECAP process has a positive effect on both strength and ductility. Moreover, the ECAP process also led to the redistribution of the second phases, as shown in Figure 4, which enhanced the role of the second phases in hindering dislocation migration and grain boundary migration, resulting in a increased second phase strengthening. Similarly, the dispersion properties of the β-TCP particle was improved by the ECAP-induced redistribution, which could contribute to an increased strengthening efficiency of β-TCP in the ECAP-processed 1β-TCP/Mg-3Zn-0.2Ca composites. Furthermore, texture plays a vital role in the mechanical properties of materials with strong textures [41]. According to the Figure 7, the single texture with the (0 0 0 1) basal plane paralleled to ED-axis was confirmed in the C-as-extruded. This kind of texture is not conducive to basal slip during the compressive deformation, but the basal slip possessed the lowest activated energy in the slip system of magnesium alloy, thereby resulting in a relatively low ductility [42]. On the contrary, after the ECAP process, a new texture component was confirmed in Figure 7b. The new texture component indicates the normal direction of the (0 0 0 1) basal plane inclines to the ED-axis by about 60 degrees. Such a texture component facilitated the activation of the basal slip system resulting in improved ductility.

Consequently, the evolution in the mechanical properties of Mg-3Zn-0.2Ca alloy and 1β-TCP/Mg-3Zn-0.2Ca composites with multiple ECAP passes depend on the synergistic effect factors, including grain refinement, second phases, β-TCP particles, and texture transformation. With the further increasing ECAP passes, the effect of grain refinement and second phases redistribution had a much higher impact on the resulting mechanical properties than the texture transformation, resulting in the increase in both strength and strain at failure of Mg-3Zn-0.2Ca alloy and 1β-TCP/Mg-3Zn-0.2Ca within six (including six) ECAP passes and reached peak values at six passes. However, the ECAP process resulted in excessive grain growth of the C-8 P-593K, which deteriorated the comprehensive mechanical properties of Mg-3Zn-0.2Ca alloy and 1β-TCP/Mg-3Zn-0.2Ca composites.

3.5. Electrochemical Analysis

Figure 9 shows the potentiodynamic polarization curves of Mg-3Zn-0.2Ca alloy and 1β-TCP/Mg-3Zn-0.2Ca composite with different ECAP passes (0, 2, 4, 6, and 8) at 593 K, and the corrosion parameters of the polarization test are shown in Table 3.

According to Table 3, the A-2 P-593 K possesses higher corrosion resistance than that of A-as-extruded, while the corrosion resistance of Mg-3Zn-0.2Ca alloy decreases with the further increased ECAP passes. Similarly, according to the electrochemical analysis results of the ECAP-processed 1β-TCP/Mg-3Zn-0.2Ca composites, the C-2 P-593 K exhibited enhanced corrosion resistance compared to the C-as-extruded. Nevertheless, when the ECAP passes are higher than two, the corrosion resistance was trending downward.

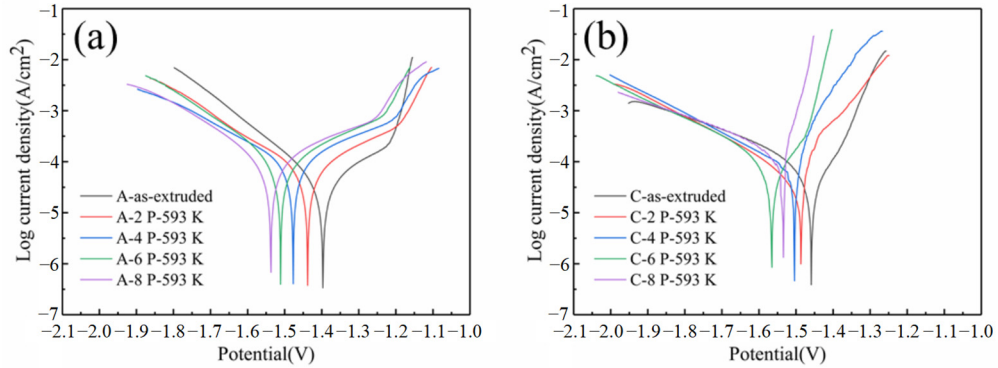

Figure 9. Potentiodynamic polarization curves of samples with different ECAP processing parameters in SBF.

Table 3. Corrosion parameters of the experimental specimens obtained from polarization curves.

Name	E_{corr} (V vs. SCE)	I_{corr} (μA·cm^{-2})	V_{corr} (mm·Y^{-1})
A-as-extruded	−1.398	53.6	1.224
C-as-extruded	−1.458	71.6	1.635
A-2 P-593 K	−1.438	39.2	0.895
C-2 P-553 K	−1.486	48.9	1.117
A-4 P-593 K	−1.478	60.3	1.377
C-4 P-593 K	−1.505	69.2	1.580
A-6 P-593 K	−1.513	78.5	1.793
C-6 P-593 K	−1.529	93.1	2.126
A-8 P-593 K	−1.566	91.2	2.083
C-8 P-593 K	−1.534	112.6	2.571

The evolution in corrosion resistance of Mg-3Zn-0.2Ca alloy and 1β-TCP/Mg-3Zn-0.2Ca composite with multiple ECAP passes could be explained from two aspects. The grain refinement has a significant impact on corrosion resistance. A protective surface film composed of MgO formed during corrosion, which could improve the corrosion resistance of matrix alloy. However, the free volume mismatch between surface film and metal matrix caused tensile stress in the surface film, thus increasing its cracking tendency. The grain refinement reduced the mismatch between the protective surface film and the underlying matrix alloy, thereby reducing the crack potential. Moreover, the ECAP process also contributes to the redistribution of the second phases and β-TCP particles in the experimental materials, which ameliorate the homogeneity and corrosion resistance of ECAP-processed materials [43]. A similar phenomenon was reported by several studies about the ECAP-processed Mg-based alloys [44,45].

Therefore, the evolution in corrosion resistance of Mg-3Zn-0.2Ca alloy and 1β-TCP/Mg-3Zn-0.2Ca composite with multiple ECAP passes depends on the synergistic effect of the above three factors (grain size, redistribution of second phases and β-TCP particles, lattice defects). For the specimens processed by ECAP with a few passes (less than two passes), the positive effect of grain refinement and redistribution of the second phase β-TCP particles on the corrosion resistance were dominant factors and exceeded the opposite effect of the increased residual stress. With the increase in ECAP passes, the negative effect of the lattice defects became the dominant factor for the corrosion behavior of experimental specimens. Hence, thus, the more ECAP passes correlate with the lower corrosion resistance.

3.6. Cell Biocompatibility

From the viewpoint of mechanical performance, A-6 P-593 K and C-6 P-593 K samples with optimized mechanical properties in each group were selected for cell biocompatibility evaluation. Figure 10 shows the relative proliferation rate (RGR) of mouse fibroblasts (L-929 cells) cultured in extracts of the A-6 P-593 K and the C-6 P-593 K specimens for 1 day, 3 days,

and 5 days. The result shows that A-6 P-593 K and C-6 P-593 K exhibit non-cytotoxicity to L-929 cells. Moreover, it is worth mentioning that C-6 P-593 K exhibited higher RGR compared to the A-6 P-593 K with the same incubation times, indicating the positive effect of β-TCP addition on the cytocompatibility of the experimental composites.

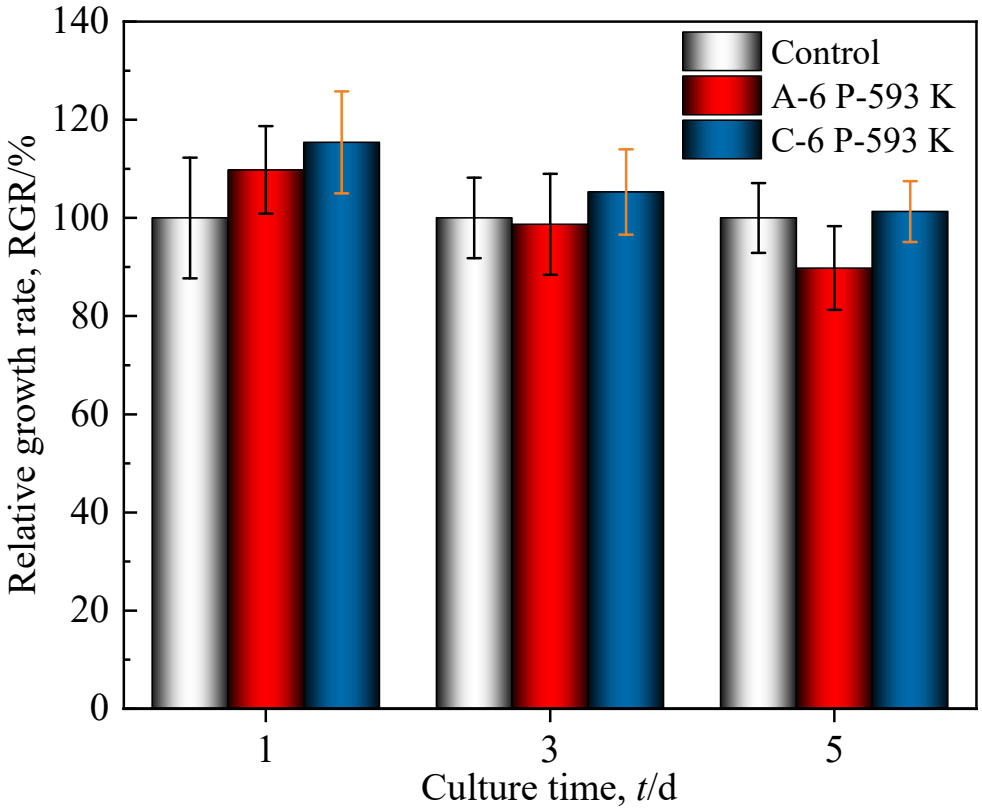

Figure 10. The relative growth rate (RGR) of L929 cells cultured with extracts of A-6 P-593 K and C-6 P-593 K specimens.

4. Conclusions

In summary, this study reported the microstructure, mechanical performance, corrosion behavior, and cytotoxicity of Mg-3Zn-0.2Ca alloy and 1β-TCP/Mg-3Zn-0.2Ca composites processed by hot extrusion combined with subsequent multi-pass ECAP process. The main findings are summarized as follows:

(1) From the viewpoint of grain refinement, hot extrusion combined with six ECAP passes at 593 K is the optimized route, resulting in an average grain size of 13.4 ± 0.6 μm and 9.6 ± 0.3 μm in Mg-3Zn-0.2Ca alloy and 1β-TCP/Mg-3Zn-0.2Ca composite, respectively. The redistribution of second phases, as well as β-TCP particles induced by the ECAP process, were also confirmed.

(2) Due to the synergistic effect of grain refinement, redistribution of second phases and β-TCP particles, and texture transformation, C-6 P-593 K displays the best mechanical properties, including the UCS of 405.3 ± 7.4 MPa, UYS of 118.9 ± 7.0 MPa and strain at failure of 10.1 ± 2.8%.

(3) For Mg-3Zn-0.2Ca alloy, the A-2 P-593 K exhibited the lowest degradation rate of 0.895 mm·Y^{-1}. The improvement of corrosion resistance is associated with the grain refinement and the uniform distribution of the second phases after the ECAP process.

(4) The cell biocompatibility result shows that the A-6 P-593 K and C-6 P-593 K had no significant cytotoxicity to L929 cells, and the addition of β-TCP could improve the cell biocompatibility. C-6 P-593 K exhibited great potential for applications in the fields of bone repair and bone replacement.

Author Contributions: X.S.: Conceptualization, Project administration, Resources, Validation, Writing—original draft, Formal analysis, Methodology, Writing—review and editing. Y.S.: Data curation, Resources, Formal analysis, Methodology, Writing—review and editing. Y.H.: Validation, Formal analysis, Writing—review and editing. M.C.: Conceptualization, Formal analysis, Methodology, Writing—review and editing. D.L.: Conceptualization, Supervision, Funding acquisition, Project administration, Formal analysis, Methodology, Writing—review and editing. All authors have read and agreed to the published version of the manuscript.

Funding: This research was funded by the National Natural Science Foundation of China (U1764254 and 51871166), Tianjin Natural Science Foundation (20JCYBJC00620).

Institutional Review Board Statement: Not applicable.

Informed Consent Statement: Not applicable.

Data Availability Statement: The raw and processed data required to reproduce these findings cannot be shared at this time as the data also forms part of an ongoing study.

Conflicts of Interest: The authors declare that they have no conflict of interest.

References

1. Wang, J.; Ma, Y.; Guo, S.; Jiang, W.; Liu, Q. Effect of Sr on the Microstructure and Biodegradable Behavior of Mg–Zn–Ca-Mn Alloys for Implant Application. *Mater. Des.* **2018**, *153*, 308–316. [CrossRef]
2. Roche, V.; Koga, G.Y.; Matias, T.B.; Kiminami, C.S.; Bolfarini, C.; Botta, W.J.; Nogueira, R.P.; Jorge Junior, A.M. Degradation of Biodegradable Implants: The Influence of Microstructure and Composition of Mg-Zn-Ca Alloys. *J. Alloy. Compd.* **2019**, *774*, 168–181. [CrossRef]
3. Chen, S.; Yao, Z.; Guan, Y.; Yang, H.; Shahzad, M.B.; Wu, Y.; Zhang, B.; Shen, L.; Yang, K. High Nitrogen Stainless Steel Drug-Eluting Stent-Assessment of Pharmacokinetics and Preclinical Safety In Vivo. *Bioact. Mater.* **2020**, *5*, 779–786. [CrossRef] [PubMed]
4. Bansal, P.; Singh, G.; Sidhu, H.S. Investigation of Corrosion Behavior and Surface Properties of Plasma Sprayed HA/Sr Reinforced Coatings on CoCr Alloys. *Mater. Chem. Phys.* **2020**, *253*, 123330. [CrossRef]
5. Lu, Y.; Turner, R.; Brooks, J.; Basoalto, H. Microstructural Characteristics and Computational Investigation on Electron Beam Welded Ti-6Al-4 V Alloy. *J. Mater. Processing Technol.* **2021**, *288*, 116837. [CrossRef]
6. Meng, X.; Jiang, Z.; Zhu, S.; Guan, S. Effects of Sr Addition on Microstructure, Mechanical and Corrosion Properties of Biodegradable Mg–Zn–Ca Alloy. *J. Alloy. Compd.* **2020**, *838*, 15561. [CrossRef]
7. Zhao, D.; Witte, F.; Lu, F.; Wang, J.; Li, J.; Qin, L. Current Status on Clinical Applications of Magnesium-Based Orthopaedic Implants: A Review from Clinical Translational Perspective. *Biomaterials* **2017**, *112*, 287–302. [CrossRef]
8. Han, H.S.; Loffredo, S.; Jun, I.; Edwards, J.; Kim, Y.C.; Seok, H.K.; Witte, F.; Mantovani, D.; Glyn-Jones, S. Current Status and Outlook on the Clinical Translation of Biodegradable Metals. *Mater. Today* **2019**, *23*, 57–71. [CrossRef]
9. Pulido-González, N.; Torres, B.; García-Rodríguez, S.; Rodrigo, P.; Bonache, V.; Hidalgo-Manrique, P.; Mohedano, M.; Rams, J. Mg–1Zn–1Ca Alloy for Biomedical Applications. Influence of the Secondary Phases on the Mechanical and Corrosion Behaviour. *J. Alloy. Compd.* **2020**, *831*, 154735. [CrossRef]
10. Zareian, Z.; Emamy, M.; Malekan, M.; Mirzadeh, H.; Kim, W.J.; Bahmani, A. Tailoring the Mechanical Properties of Mg–Zn Magnesium Alloy by Calcium Addition and Hot Extrusion Process. *Mater. Sci. Eng. A* **2020**, *774*, 138929. [CrossRef]
11. Fang, H.; Wang, C.; Zhou, S.; Zheng, Z.; Lu, T.; Li, G.; Tian, Y.; Suga, T. Enhanced Adhesion and Anticorrosion of Silk Fibroin Coated Biodegradable Mg-Zn-Ca Alloy via a Two-Step Plasma Activation. *Corros. Sci.* **2020**, *168*, 108466. [CrossRef]
12. Ding, P.; Liu, Y.; He, X.; Liu, D.; Chen, M. In Vitro and in Vivo Biocompatibility of Mg–Zn–Ca Alloy Operative Clip. *Bioact. Mater.* **2019**, *4*, 236–244. [CrossRef] [PubMed]
13. Höhn, S.; Virtanen, S.; Boccaccini, A.R. Protein Adsorption on Magnesium and Its Alloys: A Review. *Appl. Surf. Sci.* **2019**, *464*, 212–219. [CrossRef]
14. Abdel-Gawad, S.A.; Shoeib, M.A. Corrosion Studies and Microstructure of Mg−Zn−Ca Alloys for Biomedical Applications. *Surf. Interfaces* **2019**, *14*, 108–116. [CrossRef]
15. Li, J.X.; Zhang, Y.; Li, J.Y.; Xie, J.X. Effect of Trace HA on Microstructure, Mechanical Properties and Corrosion Behavior of Mg-2Zn-0.5Sr Alloy. *J. Mater. Sci. Technol.* **2018**, *34*, 299–310. [CrossRef]
16. Shahin, M.; Munir, K.; Wen, C.; Li, Y. Magnesium-Based Composites Reinforced with Graphene Nanoplatelets as Biodegradable Implant Materials. *J. Alloy. Compd.* **2020**, *828*, 15446. [CrossRef]
17. Zhao, Z.; Bai, P.; Du, W.; Liu, B.; Pan, D.; Das, R.; Liu, C.; Guo, Z. An Overview of Graphene and Its Derivatives Reinforced Metal Matrix Composites: Preparation, Properties and Applications. *Carbon* **2020**, *170*, 302–326. [CrossRef]
18. Cui, Z.; Zhang, Y.; Cheng, Y.; Gong, D.; Wang, W. Microstructure, Mechanical, Corrosion Properties and Cytotoxicity of Beta calcium Polyphosphate Reinforced ZK61 Magnesium Alloy Composite by Spark Plasma Sintering. *Mater. Sci. Eng. C* **2019**, *99*, 1035–1047. [CrossRef]

19. Tanaka, K.; Botticelli, D.; Canullo, L.; Baba, S.; Xavier, S.P. New Bone Ingrowth into β-TCP/HA Graft Activated with Argon Plasma: A Histomorphometric Study on Sinus Lifting in Rabbits. *Int. J. Implant. Dent.* **2020**, *6*, 36. [CrossRef]
20. Pan, C.; Sun, X.; Xu, G.; Su, Y.; Liu, D. The Effects of β-TCP on Mechanical Properties, Corrosion Behavior and Biocompatibility of β-TCP/Zn-Mg Composites. *Mater. Sci. Eng. C* **2020**, *108*, 110397. [CrossRef]
21. Sun, Y.; Zhang, B.; Wang, Y.; Geng, L.; Jiao, X. Preparation and Characterization of a New Biomedical Mg-Zn-Ca Alloy. *Mater. Des.* **2012**, *34*, 58–64. [CrossRef]
22. Masoudpanah, S.M.; Mahmudi, R. The Microstructure, Tensile, and Shear Deformation Behavior of an AZ31 Magnesium Alloy after Extrusion and Equal Channel Angular Pressing. *Mater. Des.* **2010**, *31*, 3512–3517. [CrossRef]
23. Yu, X.; Li, D.; Liu, Y.; Ding, P.; He, X.; Zhao, Y.; Chen, M.; Liu, D. In Vitro and in Vivo Studies on the Degradation and Biosafety of Mg-Zn-Ca-Y Alloy Hemostatic Clip with the Carotid Artery of SD Rat Model. *Mater. Sci. Eng. C* **2020**, *115*, 111093. [CrossRef] [PubMed]
24. Ly, X.; Yang, S.; Nguyen, T. Effect of Equal Channel Angular Pressing as the Pretreatment on Microstructure and Corrosion Behavior of Micro-Arc Oxidation (MAO) Composite Coating on Biodegradable Mg-Zn-Ca Alloy. *Surf. Coat. Technol.* **2020**, *395*, 125923. [CrossRef]
25. Chen, J.X.; Zhu, X.Y.; Tan, L.L.; Yang, K.; Su, X.P. Effects of ECAP Extrusion on the Microstructure, Mechanical Properties and Biodegradability of Mg–2Zn–XGd–0.5Zr Alloys. *Acta Metall. Sin. (Engl. Lett.)* **2021**, *34*, 205–216. [CrossRef]
26. Zhuang, Y.; Wang, H.; Li, H.; Zheng, L.; Li, J.; Zhou, P. Synergistic Effect of Grain Size, β-Mg17Al12, and Texture on Mechanical Properties of Mg-15Al (Wt.%) Magnesium Alloy Processed by Equal Channel Angular Pressing. *J. Mater. Eng. Perform.* **2020**, *29*, 4360–4369. [CrossRef]
27. Prithivirajan, S.; Narendranath, S.; Desai, V. Analysing the Combined Effect of Crystallographic Orientation and Grain Refinement on Mechanical Properties and Corrosion Behaviour of ECAPed ZE41 Mg Alloy. *J. Magnes. Alloy.* **2020**, *8*, 1128–1143. [CrossRef]
28. Krywopusk, N.M.; Kecskes, L.J.; Weihs, T.P. Microstructural Characterization of Pure Mg and AZ31B Processed by ECAE. *Mater. Charact.* **2019**, *158*, 109950. [CrossRef]
29. Subramani, M.; Huang, S.J.; Borodianskiy, K. Effect of SiC Nanoparticles on AZ31 Magnesium Alloy. *Materials* **2022**, *15*, 1004. [CrossRef]
30. Huang, S.J.; Subramani, M.; Borodianskiy, K. Strength and Ductility Enhancement of AZ61/Al_2O_3/SiC Hybrid Composite by ECAP Processing. *Mater. Today Commun.* **2022**, *31*, 103261. [CrossRef]
31. Abbas, A.; Huang, S.J. ECAP Effects on Microstructure and Mechanical Behavior of Annealed WS2/AZ91 Metal Matrix Composite. *J. Alloy. Compd.* **2020**, *835*, 155466. [CrossRef]
32. Xu, Q.; Ma, A.; Saleh, B.; Li, Y.; Yuan, Y.; Jiang, J.; Ni, C. Enhancement of Strength and Ductility of SiCp/AZ91 Composites by RD-ECAP Processing. *Mater. Sci. Eng. A* **2020**, *771*, 138579. [CrossRef]
33. Xu, B.; Sun, J.; Yang, Z.; Xiao, L.; Zhou, H.; Han, J.; Liu, H.; Wu, Y.; Yuan, Y.; Zhuo, X.; et al. Microstructure and Anisotropic Mechanical Behavior of the High-Strength and Ductility AZ91 Mg Alloy Processed by Hot Extrusion and Multi-Pass RD-ECAP. *Mater. Sci. Eng. A* **2020**, *780*, 139191. [CrossRef]
34. Gan, W.M.; Wu, K.; Zheng, M.Y.; Wang, X.J.; Chang, H.; Brokmeier, H.G. Microstructure and Mechanical Property of the ECAPed Mg2Si/Mg Composite. *Mater. Sci. Eng. A* **2009**, *516*, 283–289. [CrossRef]
35. Zheng, H.R.; Li, Z.; You, C.; Liu, D.B.; Chen, M.F. Effects of MgO Modified β-TCP Nanoparticles on the Microstructure and Properties of β-TCP/Mg-Zn-Zr Composites. *Bioact. Mater.* **2017**, *2*, 1–9. [CrossRef]
36. Liu, J.; Li, J.; Xu, C. Interaction of the Cutting Tools and the Ceramic-Reinforced Metal Matrix Composites during Micro-Machining: A Review. *CIRP J. Manuf. Sci. Technol.* **2014**, *7*, 55–70. [CrossRef]
37. Casati, R.; Vedani, M. Metal Matrix Composites Reinforced by Nano-Particles—A Review. *Metals* **2014**, *4*, 65–83. [CrossRef]
38. Zhou, D.; Qiu, F.; Wang, H.; Jiang, Q. Manufacture of Nano-Sized Particle-Reinforced Metal Matrix Composites: A Review. *Acta Metall. Sin. (Engl. Lett.)* **2014**, *27*, 798–805. [CrossRef]
39. Reddy, M.P.; Shakoor, R.A.; Parande, G.; Manakari, V.; Ubaid, F.; Mohamed, A.M.A.; Gupta, M. Enhanced Performance of Nano-Sized SiC Reinforced Al Metal Matrix Nanocomposites Synthesized through Microwave Sintering and Hot Extrusion Techniques. *Prog. Nat. Sci. Mater. Int.* **2017**, *27*, 606–614. [CrossRef]
40. Orlov, D.; Ralston, K.D.; Birbilis, N.; Estrin, Y. Enhanced Corrosion Resistance of Mg Alloy ZK60 after Processing by Integrated Extrusion and Equal Channel Angular Pressing. *Acta Mater.* **2011**, *59*, 6176–6186. [CrossRef]
41. Yin, S.M.; Wang, C.H.; Diao, Y.D.; Wu, S.D.; Li, S.X. Influence of Grain Size and Texture on the Yield Asymmetry of Mg-3Al-1Zn Alloy. *J. Mater. Sci. Technol.* **2011**, *27*, 29–34. [CrossRef]
42. Kim, W.J.; Hong, S.I.; Kim, Y.S.; Min, S.H.; Jeong, H.T.; Lee, J.D. Texture Development and Its Effect on Mechanical Properties of an AZ61 Mg Alloy Fabricated by Equal Channel Angular Pressing. *Acta Mater.* **2003**, *51*, 3293–3307. [CrossRef]
43. Kirkland, N.T.; Lespagnol, J.; Birbilis, N.; Staiger, M.P. A Survey of Bio-Corrosion Rates of Magnesium Alloys. *Corros. Sci.* **2010**, *52*, 287–291. [CrossRef]
44. Song, D.; Ma, A.; Jiang, J.; Lin, P.; Yang, D.; Fan, J. Corrosion Behavior of Equal-Channel-Angular-Pressed Pure Magnesium in NaCl Aqueous Solution. *Corros. Sci.* **2010**, *52*, 481–490. [CrossRef]
45. Song, D.; Ma, A.B.; Jiang, J.H.; Lin, P.H.; Yang, D.H.; Fan, J.F. Corrosion Behaviour of Bulk Ultra-Fine Grained AZ91D Magnesium Alloy Fabricated by Equal-Channel Angular Pressing. *Corros. Sci.* **2011**, *53*, 362–373. [CrossRef]